Derivation of a realistic forcing term to reproduce the turbulent characteristics of round jets on the centerline

Kyupaeck Jeff Rah*
Department of Mechanical and Civil Engineering, California Institute of Technology, California 91125, USA

Chandru Dhandapani
Graduate Aerospace Laboratories, California Institute of Technology, California 91125, USA

Guillaume Blanquart†
Department of Mechanical and Civil Engineering, California Institute of Technology, California 91125, USA

(Received 14 December 2017; published 29 August 2018)

Turbulence forcing techniques are often required in the numerical simulation of statistically stationary turbulent flows. However, the existing forcing techniques are not based on physics, but rather arbitrary numerical methods that sustain the turbulent kinetic energy. In this work, a forcing technique is devised to reproduce the centerline turbulent characteristics of round jets in a triply periodic box. It is derived from the Navier-Stokes equations by applying a Reynolds decomposition with the mean velocity of the axisymmetric jet. The result is an anisotropic linear forcing term, which is intended to be used in a three-dimensional box to create turbulence. Four direct numerical simulations with different Re_λ have been performed with these forcing terms. The budget of the terms in the kinetic energy equation is very close to the experimental measurement on the centerline. The anisotropy, kinetic energy k, and dissipation rate ε of the simulations are also comparable to experimental values. Finally, the kinetic energy spectrum in the axial direction, $\phi(\kappa_1)$, is presented. With appropriate normalizations, the spectrum agrees well with the round jet spectrum on its centerline.

DOI: 10.1103/PhysRevFluids.3.084606

I. INTRODUCTION

Turbulence, by nature, quickly loses its energy and dissipates. In numerical simulations, however, stationary turbulence is often required to obtain meaningful statistics. For instance, it is needed in the simulations of turbulent flows and scalar mixing processes in a triply periodic box [1–7]. It can also be desired in geometries other than triply periodic box; for example, Savard *et al.* [8], Poludnenko and Oran [9], and Hamlington *et al.* [10] needed statistically stationary turbulence when examining turbulent flames. In these cases, an artificial forcing scheme must be used to prevent the turbulence from decaying.

Traditional forcing schemes have been implemented in spectral space. Below is the Fourier-transformed incompressible momentum equation,

$$\frac{\partial \widehat{\boldsymbol{u}}}{\partial t} + \widehat{\boldsymbol{u}\cdot\nabla\boldsymbol{u}} = -\frac{1}{\rho}\widehat{\nabla p} + \nu\widehat{\nabla^2\boldsymbol{u}} + \widehat{\boldsymbol{f}}, \tag{1}$$

*krah@caltech.edu
†http://www.theforce.caltech.edu

where $\boldsymbol{u}$ is the velocity, ρ is density, p is pressure, and ν is kinematic viscosity. The operator $\widehat{\cdot}$ denotes a Fourier transformation. $\widehat{\boldsymbol{f}}$ is the forcing term that prevents the turbulence from decaying. In the literature, mainly three categories of forcing schemes can be found.

In the first category, a forcing term $\widehat{\boldsymbol{f}}(\boldsymbol{\kappa}, t) = c(\boldsymbol{\kappa}, t)\widehat{\boldsymbol{u}}(\boldsymbol{\kappa}, t)$ is used for certain chosen wave-number shells. For example, Ghosal *et al.* [3] and Carati *et al.* [4] applied the following forcing to all the modes in the wave-number shell $|\boldsymbol{\kappa}| \leqslant \kappa_f$:

$$\widehat{\boldsymbol{f}}(\boldsymbol{\kappa}, t) = \varepsilon \frac{\widehat{\boldsymbol{u}}(\boldsymbol{\kappa}, t)}{N|\widehat{\boldsymbol{u}}(\boldsymbol{\kappa}, t)|^2}, \tag{2}$$

where ε is the average dissipation rate, N is the number of modes in the wave-number shell, and κ_f is the maximum wave number subjected to forcing. Both simulations of Ghosal and Carati used $\kappa_f = 2\kappa_{\min}$, where $\kappa_{\min}$ is the minimum wave number determined by the domain size.

The second class of schemes maintains the energy of certain wave-number shells at a constant level for all time steps. For instance, Chasnov [5] and Sullivan *et al.* [6] kept the energy constant in the wave-number shell $|\boldsymbol{\kappa}| \leqslant \kappa_f$. Chasnov used $\kappa_f = 2\kappa_{\min}$ and Sullivan used $\kappa_f = 2\sqrt{2}\kappa_{\min}$. This method assumes that the higher wave-number flow structure should not be changed much and that the energy should pass down to the smaller scales. Seror *et al.* [7] maintained the total kinetic energy at a constant level by injecting the lost energy into the wave numbers at $|\boldsymbol{\kappa}| \leqslant 5\kappa_{\min}$ for each time step. This was achieved by forcing

$$\widehat{u}^{n+1}(\boldsymbol{\kappa}) = \sqrt{1 + \frac{\Delta E}{\int_{\kappa_{\min}}^{\kappa_{\max}} E(\kappa) d\kappa}}\, \widehat{u}^{*}(\boldsymbol{\kappa}), \tag{3}$$

where $\widehat{u}^{n+1}(\boldsymbol{\kappa})$ is the Fourier coefficient at time $(n+1)\Delta t$ for $|\boldsymbol{\kappa}| \leqslant 5\kappa_{\min}$, and $\widehat{u}^{*}(\boldsymbol{\kappa})$ is the Fourier coefficient computed by integrating the Navier-Stokes equation with $\widehat{u}^{n}(\boldsymbol{\kappa})$ as an initial condition. ΔE is the lost energy, and $\kappa_{\max} = 5\kappa_{\min}$.

Stochastic schemes have also been devised for the forcing term. Eswaran and Pope [11] developed the following expression:

$$\widehat{\boldsymbol{f}}(\boldsymbol{\kappa}, t) = \widehat{\boldsymbol{b}}(\boldsymbol{\kappa}, t) - \frac{\boldsymbol{\kappa}(\boldsymbol{\kappa} \cdot \widehat{\boldsymbol{b}}(\boldsymbol{\kappa}, t))}{\boldsymbol{\kappa} \cdot \boldsymbol{\kappa}}, \tag{4}$$

where $\widehat{\boldsymbol{b}}$ is a complex vector-valued stochastic process based on Uhlenbeck-Ornstein random process [12]. This expression is the projection of the stochastic process onto the plane normal to $\boldsymbol{\kappa}$. The forcing term is only applied for $|\boldsymbol{\kappa}| \leqslant \kappa_f$. Two values of κ_f, $\sqrt{2}\kappa_{\min}$ and $2\sqrt{2}\kappa_{\min}$, were tested for the simulations of Eswaran and Pope. Alvelius [13] also formulated a random force:

$$\widehat{\boldsymbol{f}}(\boldsymbol{\kappa}, t) = A_{\text{ran}}(\boldsymbol{\kappa}, t)\boldsymbol{e}_1(\boldsymbol{\kappa}) + B_{\text{ran}}(\boldsymbol{\kappa}, t)\boldsymbol{e}_2(\boldsymbol{\kappa}), \tag{5}$$

where $\boldsymbol{e}_1$ and $\boldsymbol{e}_2$ are unit vectors orthogonal to each other and to $\boldsymbol{\kappa}$, and A_{ran} and B_{ran} are random complex numbers determined by the prescribed force spectrum.

As shown above, there have been various forcing methods in spectral space to create statistically stationary turbulence. However, these spectral forcing schemes are not applicable to nonperiodic boundary condition cases, and it is difficult to implement in numerical simulations based on the momentum equations in physical space. Furthermore, these methods are not developed to represent any practical flows. They sustain the turbulent energy of velocity fields, yet they are rather arbitrary numerical methods.

The objective of the current study is to develop a forcing scheme to produce a turbulent flow whose characteristics resemble those of a practical flow. Any turbulent flow can be chosen as a target. In this investigation, however, we aim to reproduce the turbulence in the centerline region of fully developed turbulent round jets. In other words, the purpose is to imitate the local turbulent characteristics of axisymmetric jets at $r = 0$. It is not our goal to derive a source term for the entire region of a round jet.

The objective will be accomplished by adopting the linear forcing term of Lungdren [14]. After a review of Lundgren's forcing scheme in Sec. II, we derive our forcing method in Sec. III. The results are presented in Sec. IV.

II. REVIEW OF LUNDGREN'S LINEAR FORCING TERM AND MOTIVATION

The linear forcing scheme, suggested by Lundgren [14] and further explored by Rosales and Meneveau [15], is different from the other spectral schemes. The essential difference, as described at the end of Sec. I, is that the forcing term is applied in physical space instead of in spectral space. Since the forcing term of the current study takes a similar form, this linear method is reviewed in detail first.

Let us consider the Reynolds decomposition, $\boldsymbol{u} = \overline{\boldsymbol{u}} + \boldsymbol{u}'$, where $\overline{\boldsymbol{u}}$ is the mean velocity and $\boldsymbol{u}'$ is the fluctuating velocity. The momentum equation for the velocity fluctuation can be obtained from the original Navier-Stokes equation after subtracting the mean of the equation:

$$N(\overline{\boldsymbol{u}} + \boldsymbol{u}') - \overline{N(\overline{\boldsymbol{u}} + \boldsymbol{u}')}. \tag{6}$$

This gives

$$\frac{\partial \boldsymbol{u}'}{\partial t} + \overline{\boldsymbol{u}} \cdot \nabla \boldsymbol{u}' + \boldsymbol{u}' \cdot \nabla \overline{\boldsymbol{u}} + \boldsymbol{u}' \cdot \nabla \boldsymbol{u}' - \nabla \cdot \overline{\boldsymbol{u}'\boldsymbol{u}'} = -\frac{1}{\rho}\nabla p' + \nu \nabla^2 \boldsymbol{u}', \tag{7}$$

where N is the set of Navier-Stokes equations and p' is the pressure fluctuation. The overline $\overline{\cdot}$ denotes ensemble averaging.

The third term, $\boldsymbol{u}' \cdot \nabla \overline{\boldsymbol{u}}$, appears as an energy production term in the kinetic energy equation. Lundgren argued that since this production term is proportional to $\boldsymbol{u}'$, a source term in physical space should have the following form:

$$\boldsymbol{f} = A\boldsymbol{u}', \tag{8}$$

where A is an arbitrary constant. Then, the resultant momentum equation is

$$\frac{\partial \boldsymbol{u}'}{\partial t} + \boldsymbol{u}' \cdot \nabla \boldsymbol{u}' = -\frac{1}{\rho}\nabla p' + \nu \nabla^2 \boldsymbol{u}' + A\boldsymbol{u}'. \tag{9}$$

This isotropic source term provides a continuous energy injection at all scales, maintaining the turbulence at a statistically stationary state.

The kinetic energy equation can be derived by multiplying $\boldsymbol{u}'$ to Eq. (9):

$$\frac{\partial k}{\partial t} + \boldsymbol{u}' \cdot \nabla k = -\frac{1}{\rho}\nabla \cdot \boldsymbol{u}' p' + \nu \nabla^2 k - \varepsilon + 2Ak, \tag{10}$$

where $k = \frac{1}{2}\boldsymbol{u}' \cdot \boldsymbol{u}'$ is the kinetic energy, $\varepsilon = 2\nu S_{ij} S_{ij}$ is the energy dissipation rate, and $S_{ij} = \frac{1}{2}(\frac{\partial u_i'}{\partial x_j} + \frac{\partial u_j'}{\partial x_i})$ is the strain-rate tensor. Since spatial derivatives of the volumetric average quantities are zero for statistically homogeneous flows, the following relation can be derived:

$$\frac{\partial \langle k \rangle}{\partial t} = -\langle \varepsilon \rangle + 2A\langle k \rangle, \tag{11}$$

where $\langle \cdot \rangle$ is the volumetric averaging. In homogeneous flows, volume averaging is equivalent to ensemble averaging. Then, it follows that A determines the ratio of the average turbulent kinetic energy to the average energy dissipation rate for statistically stationary turbulence; i.e.,

$$A = \frac{\langle \varepsilon \rangle}{2\langle k \rangle}. \tag{12}$$

Lundgren examined one term in Eq. (7) and proposed a generic expression, $\boldsymbol{f} = A\boldsymbol{u}'$, for the forcing term in Eq. (8). However, all the terms in Eq. (7) could be examined by using mean velocity information of practical turbulent flows.

III. PROPOSED FORCING TERM

The new forcing term is meant to replicate the turbulent characteristics of round jets in a triply periodic cubic box, in which the flow is statistically homogeneous with zero mean velocity. A periodic geometry is convenient to compute statistics and perform spectral analyses.

A. Review of turbulent jets

A typical turbulent jet consists of three zones: the potential core, the transition zone, and the fully developed self-similar zone. The velocity in the self-similar zone can be expressed as a function of the centerline velocity, U_c, and the similarity variable, $\eta = r/x$, where r is the radial distance and x is the axial distance. It has been shown that U_c scales as $1/x$ in the self-similar region by many experiments [16–20].

Abramovich [21] and Pope [16] used a stream function theory to describe the mean velocity of axisymmetric turbulent jets. The result is shown below:

$$\overline{u}_x = U_c \frac{F'(\eta)}{\eta}, \tag{13}$$

$$\overline{u}_r = U_c \left[F'(\eta) - \frac{1}{\eta} F(\eta) \right], \tag{14}$$

where $F(\eta)$ is a function to be determined. Abramovich and Pope used different expressions for $F(\eta)$ to fit the experimental velocity profiles. However, the two expressions yield the same velocity gradient matrix, when evaluated at the centerline of a certain location x_o:

$$\boldsymbol{\nabla} \overline{\boldsymbol{u}}(x = x_o, \eta = 0) = \begin{bmatrix} -\frac{U_c}{x_o} & 0 & 0 \\ 0 & \frac{1}{2}\frac{U_c}{x_o} & 0 \\ 0 & 0 & \frac{1}{2}\frac{U_c}{x_o} \end{bmatrix}. \tag{15}$$

In the self-similar region, the fluctuating velocity is also a function of the centerline velocity and the similarity variable only. More important,

$$\sqrt{\langle u_i'^2 \rangle} = U_c f_i(\eta), \tag{16}$$

as demonstrated by many experiments [16–20]. Thus, $\sqrt{\langle u_i'^2 \rangle}/U_c$ must only be a function of η. The summation convention over repeated indices is not adopted here.

B. Derivation of the forcing term

Theoretically, Eqs. (13)–(15) can be applied to Eq. (7), to remove the $\overline{\boldsymbol{u}}$ terms and obtain the momentum equation for the fluctuating velocities. However, the resulting turbulent flow would not be statistically homogeneous; indeed, $\boldsymbol{u}'$ decreases as $1/x$ in a turbulent jet. It is thus preferable to normalize first $\boldsymbol{u}'$ with x/x_o. Then,

$$\boldsymbol{u}^* = \frac{x}{x_o}\boldsymbol{u}' = \frac{x}{x_o}(\boldsymbol{u} - \overline{\boldsymbol{u}}), \tag{17}$$

where $\boldsymbol{u}$ is the original velocity of the jet, and the asterisk * denotes the normalized quantity. With this normalization, the continuity equation, when evaluated at $x = x_o$, would have a nonzero term on the right-hand side as below:

$$\boldsymbol{\nabla} \cdot \boldsymbol{u}^* = \frac{u_x^*}{x_o}. \tag{18}$$

Although it is possible to perform a numerical simulation with an extra term in the continuity equation, it is preferred not to, for practical reasons. Thus, we propose the following normalization in lieu of

Eq. (17):

$$u_x^* = \frac{x}{x_o}(u_x - \overline{u}_x)\exp\left(1 - \frac{x}{x_o}\right), \quad u_i^* = \frac{x}{x_o}(u_i - \overline{u}_i). \tag{19}$$

u_i denotes either of the transverse velocities.

Now, Eqs. (13)–(15) and (19) can be applied to Eq. (7). The terms are evaluated on the centerline at a certain location x_o, leading to the following equations:

(1) Continuity:

$$\nabla \cdot \boldsymbol{u}^* = 0. \tag{20}$$

(2) Longitudinal direction:

$$\frac{Du_x^*}{Dt} + \boldsymbol{u}^* \cdot \nabla u_x^* + \frac{1}{\rho}\frac{\partial p}{\partial x} - \nu\nabla^2 u_x^* = \nabla \cdot \overline{\boldsymbol{u}^* u_x^*} + \nu\frac{u_x^*}{x_o^2} + \frac{U_c}{x_o}u_x^*. \tag{21}$$

(3) Transverse directions:

$$\begin{aligned}&\frac{Du_i^*}{Dt} + \boldsymbol{u}^* \cdot \nabla u_i^* + \frac{1}{\rho}\frac{\partial p}{\partial x_i} - \nu\nabla^2 u_i^*. \\ &= \nabla \cdot \overline{\boldsymbol{u}^* u_i^*} + \nu\left[2\frac{u_i^*}{x_o^2} - \frac{2}{x_o}\frac{\partial u_i^*}{\partial x}\right] - \frac{\overline{u_x^* u_i^*}}{x_o} + \frac{u_x^* u_i^*}{x_o} + \frac{1}{2}\frac{U_c}{x_o}u_i^*.\end{aligned} \tag{22}$$

The vector notation applies to all three directions, and u_i^* and x_i apply to either of the transverse directions. The material derivative is defined as $\frac{D}{Dt} \equiv \frac{\partial}{\partial t} + U_c\frac{\partial}{\partial x}$, which provides the effect of a Galilean transformation. This $\frac{D}{Dt}$ will be used as the time derivative in the computations.

Several terms on the right-hand side (RHS) of Eqs. (21) and (22) are negligible, as compared to the other terms. First, $\nu u_i^*/x_o^2 \ll U_c u_i^*/x_o$ for high-Reynolds-number flows. In fact, the ratio $U_c x_o/\nu$ is proportional to the jet Reynolds number $\mathrm{Re}_D = U_o D/\nu$, based on the exit nozzle velocity, U_o, and the nozzle diameter, D [21]. Similarly, $\frac{\nu}{x_o}\frac{\partial u_i^*}{\partial x} \ll \boldsymbol{u}^* \cdot \nabla u_i^*$. The ratio of the two terms is of the same magnitude as the local turbulent Reynolds number. In addition, $\nabla \cdot \overline{\boldsymbol{u}^* u_i^*}$ and $\overline{u_x^* u_i^*}/x_o$ appear as $\overline{u_i^*}\nabla \cdot \overline{\boldsymbol{u}^* u_i^*}$ and $\overline{u_i^*}\,\overline{u_x^* u_i^*}/x_o$, respectively, in the kinetic energy equation. They do not contribute to the mean kinetic energy, because $\overline{u_i^*} \equiv 0$. $u_x^* u_i^*/x_o$, on the other hand, appears as $\overline{u_x^* u_i^{*2}}/x_o$ in the kinetic energy equation. The magnitude of $\overline{u_x^* u_i^{*2}}/x_o$ can be compared to that of $\frac{1}{2}\frac{U_c}{x_o}\overline{u_i^{*2}}$. According to experiments [19,20,22], the value of $\overline{u_x' u_i'^2}/U_c^3$ is 0.0010–0.0017, and that of $\overline{u_i'^2}/U_c^2$ is 0.036–0.050. Then, the ratio of $\overline{u_x' u_i'^2}/x_o$ to $\frac{1}{2}\frac{U_c}{x_o}\overline{u_i'^2}$ ranges from 0.040 to 0.094. Although the governing equations are for the normalized quantities, u_i^*, we will assume here that turbulent parameters of u_i^* are comparable to those of u_i'. Thus, we will conclude that $u_x^* u_i^*/x_o$ is also negligible. With these simplifications, the only terms significantly contributing to the production of kinetic energy are $\frac{U_c}{x_o}u_x^*$ in Eq. (21) and $\frac{1}{2}\frac{U_c}{x_o}u_i^*$ in Eq. (22). Thus, only these RHS terms in the momentum equations are retained; the other terms are removed.

The final governing equations for $\boldsymbol{u}^*$ are as follows:

(1) Continuity:

$$\nabla \cdot \boldsymbol{u}^* = 0. \tag{23}$$

(2) Longitudinal direction:

$$\frac{Du_x^*}{Dt} + \boldsymbol{u}^* \cdot \nabla u_x^* + \frac{1}{\rho}\frac{\partial p}{\partial x} - \nu\nabla^2 u_x^* = \frac{U_c}{x_o}u_x^*. \tag{24}$$

(3) Transverse directions:

$$\frac{Du_i^*}{Dt} + \boldsymbol{u}^* \cdot \nabla u_i^* + \frac{1}{\rho}\frac{\partial p}{\partial x_i} - \nu\nabla^2 u_i^* = \frac{1}{2}\frac{U_c}{x_o}u_i^*. \tag{25}$$

TABLE I. Sources of the forcing term.

	Mean flow	Advection normalization	Continuity normalization
Longitudinal	$\frac{U_c}{x_o}u_x^*$	$\frac{U_c}{x_o}u_x^*$	$-\frac{U_c}{x_o}u_x^*$
Transverse	$-\frac{1}{2}\frac{U_c}{x_o}u_i^*$	$\frac{U_c}{x_o}u_i^*$	0

(4) Ensemble-averaged kinetic energy:

$$\frac{D\langle k^*\rangle}{Dt} = -\langle\varepsilon^*\rangle + \frac{U_c}{x_o}\left\langle k^* + \frac{u_x^{*2}}{2}\right\rangle, \tag{26}$$

where $\langle\varepsilon^*\rangle = 2\nu\langle S_{ij}^* S_{ij}^*\rangle = \nu\langle\frac{\partial u_i^*}{\partial x_j}\frac{\partial u_i^*}{\partial x_j}\rangle$ is the energy dissipation rate, and $S_{ij}^* = \frac{1}{2}(\frac{\partial u_i^*}{\partial x_j} + \frac{\partial u_j^*}{\partial x_i})$ is the strain-rate tensor. It is important to note that the magnitude of the source terms is determined by two simple experimental parameters, U_c and x_o.

The sources of this forcing term are summarized below:

(1) Longitudinal direction:

$$\text{Production}: \quad -\boldsymbol{u'}\cdot\nabla\overline{u}_x|_{x=x_o} = \frac{U_c}{x_o}\frac{x_o}{x}e^{\frac{x}{x_o}-1}u_x^*\bigg|_{x=x_o} = \frac{U_c}{x_o}u_x^*, \tag{27}$$

$$\text{Advection}: \quad -\overline{\boldsymbol{u}}\cdot\nabla u_x'|_{x=x_o} = -U_c\frac{\partial}{\partial x}\left(\frac{x_o}{x}e^{\frac{x}{x_o}-1}u_x^*\right)\bigg|_{x=x_o} = \frac{U_c}{x_o}u_x^* - \frac{U_c}{x_o}u_x^* - \cancel{U_c\frac{\partial u_x^*}{\partial x}}. \tag{28}$$

(2) Transverse directions:

$$\text{Production}: \quad -\boldsymbol{u'}\cdot\nabla\overline{u}_i|_{x=x_o} = -\frac{1}{2}\frac{U_c}{x_o}\frac{x_o}{x}u_i^*\bigg|_{x=x_o} = -\frac{1}{2}\frac{U_c}{x_o}u_i^*, \tag{29}$$

$$\text{Advection}: \quad -\overline{\boldsymbol{u}}\cdot\nabla u_i'|_{x=x_o} = -U_c\frac{\partial}{\partial x}\left(\frac{x_o}{x}u_i^*\right)\bigg|_{x=x_o} = \frac{U_c}{x_o}u_i^* - \cancel{U_c\frac{\partial u_i^*}{\partial x}}. \tag{30}$$

The $U_c\frac{\partial u_i^*}{\partial x}$ terms do not appear in the governing equations, as they are combined with $\frac{\partial u_i^*}{\partial t}$ to make $\frac{Du_i^*}{Dt}$.

Essentially, the source term from *production* is generated by the gradient of the mean flow, $\nabla\overline{\boldsymbol{u}}$. The source term from *advection*, on the other hand, is generated by two normalizations, $\frac{x_o}{x}$ and the exponential one. Since $\boldsymbol{u}'$ decreases as the mean flow travels in x direction, the $\frac{x_o}{x}$ normalization is intended to convert this advection effect into a source term. Thus, this normalization will be called *advection normalization*. The $e^{(x/x_o-1)}$ normalization is a mathematical technique to remove the extra source term in the continuity equation, Eq. (18). This will be called *continuity normalization*. All three contributions are summarized in Table I.

The source terms from the mean flow make this forcing scheme seem as simulating an axisymmetric expansion, but the two normalizations are essential to the derivation. The first normalization takes into account the decrease of $\boldsymbol{u}'$ along the axial direction, and the second one maintains its continuity. The source terms from the two normalizations, with a combination with the mean flow terms, create turbulence in a three-dimensional (3D) box that is similar to the centerline of a round jet.

C. Properties of the forcing scheme

Three key observations must be made about the derived forcing scheme.

First, this current forcing term is the result of applying the physical laws of a practical turbulent flow. The other forcing schemes introduced in Sec. I did not directly reflect the physical situations, but

rather devised some arbitrary numerical methods to maintain the turbulence. Even Lundgren's linear forcing scheme introduced in Sec. II was theoretical; it was not specific to any flow configurations. The isotropic turbulence generated by this forcing is not close to any practical types of flows. In the present derivation, on the other hand, the physics of a practical flow is considered.

Second, the resultant source term is a linear forcing term. It may have been expected from the form of the term $\boldsymbol{u}' \cdot \nabla \overline{\boldsymbol{u}}$ that the source term should be linear, but the additional normalizations also yield linear terms. Also, this new source term is a forcing term in physical space, not in spectral space. This physical forcing also injects energy throughout all the scales. It is essentially different from other spectral forcing schemes that often restrict the energy injection to narrow wave-number regions.

Third, the forcing term is anisotropic; it is twice as strong in one direction as in the other directions. Lundgren's forcing term is also linear, but it is isotropic. Real flows rarely approach isotropy at the large scale. The anisotropic forcing in the current study is qualitatively consistent with the anisotropy of turbulent jets, in which the fluctuating velocity is stronger in one direction.

D. *A priori* analysis and simulation procedure

As detailed in Ref. [2], for triply periodic direct numerical simulations (DNS) with Lundgren's linear source term in physical space, the average values of some turbulent parameters, such as the kinetic energy k and the dissipation rate ε, can be predicted by analyzing the kinetic energy equation. The same analysis is applied to the current investigation.

First, by applying the condition of statistical stationarity ($\frac{\partial}{\partial t} = 0$) on the kinetic energy equation, Eq. (26) reduces to

$$\langle \varepsilon^* \rangle = \frac{U_c}{x_o} \left\langle k^* + \frac{u_x^{*2}}{2} \right\rangle. \tag{31}$$

It shows the balance between energy dissipation and energy production.

Let k_o and ε_o denote the expected values for the kinetic energy and dissipation rate, respectively. Also, the integral length scale is defined as

$$l \equiv \frac{(\langle \boldsymbol{u}' \cdot \boldsymbol{u}' \rangle / 3)^{3/2}}{\varepsilon_o} = \frac{\left(\frac{2}{3} k_o\right)^{3/2}}{\varepsilon_o}. \tag{32}$$

Using this definition with Eq. (31), k_o and ε_o may be expressed as

$$k_o = \frac{27}{8} \frac{U_c^2}{x_o^2} \left(1 + \frac{\langle u_x^{*2} \rangle}{\langle \boldsymbol{u}^{*2} \rangle} \right)^2 l^2 \tag{33}$$

and

$$\varepsilon_o = \frac{27}{8} \frac{U_c^3}{x_o^3} \left(1 + \frac{\langle u_x^{*2} \rangle}{\langle \boldsymbol{u}^{*2} \rangle} \right)^3 l^2, \tag{34}$$

where U_c and x_o are input values related to a particular experimental setup. The ratio $\langle u_x^{*2} \rangle / \langle \boldsymbol{u}^{*2} \rangle$ and the integral length scale are outputs of the numerical simulations, which are unknown *a priori*. As will be shown later in Sec. IV B, they are found to be constant across a wide range of Reynolds numbers and given by

$$l \approx 0.24 L, \tag{35}$$

$$\frac{\langle u_x^{*2} \rangle}{\langle \boldsymbol{u}^{*2} \rangle} \approx 0.49, \tag{36}$$

where L is the computational domain width. The integral length scale evaluated from any 3D box of turbulence is a function of the box size, and the ratio of l to L is determined by the forcing term.

Rosales and Meneveau [15] found that $l \approx 0.19L$, when Lundgren's linear forcing term is used. For spectral methods, l/L ranges from 0.15 to 0.30.

It is well accepted that the integral length scale is proportional to the downstream distance. According to Pope [16], $l \approx 0.0962x_o$ in a turbulent jet experiment. However, it should be noted that this approximation varies by experiments, mainly due to the different estimations of ε, as later shown in Sec. IV D. In this study, $l = 0.0962x_o$ is used to determine the domain width. Since we want the periodic DNS to have the same integral length scale as the experiments, we should set the size of the computational domain as

$$L = 0.399x_o. \tag{37}$$

The procedure of conducting the DNS in the current investigation can be summarized as follows:

(1) Find the centerline velocity U_c and the axial location x_o of the target experiment.
(2) Use the ratio of U_c and x_o to determine the source term for the DNS.
(3) Use x_o to determine the length of the DNS cubic box, as $L = 0.399x_o$.
(4) Perform the DNS in a triply periodic configuration.

These various *a priori* values are compared against actual values from turbulent jet experiments and simulations in Sec. IV D.

E. Reynolds numbers

The root-mean-square velocity fluctuation, u_{rms}, the Taylor microscale, λ, and the Taylor-microscale Reynolds number, Re_λ, are defined as

$$u_{\text{rms}} = \sqrt{\frac{2k}{3}}, \tag{38}$$

$$\lambda = \sqrt{15\frac{\nu}{\varepsilon}}u_{\text{rms}}, \tag{39}$$

$$\text{Re}_\lambda = \frac{\lambda u_{\text{rms}}}{\nu}. \tag{40}$$

The entire turbulent flow can be represented by Re_λ. Once appropriate normalizations are applied to the dimensional parameters, Re_λ is the only free input parameter for the triply periodic DNS [2,15]. Re_λ can also be predicted *a priori*, as k_o and ε_o are predicted in Sec. III D:

$$\text{Re}_\lambda^o = \sqrt{\frac{45}{2\nu}\frac{U_c}{x_o}\left(1 + \frac{\langle u_x^{*2}\rangle}{\langle \boldsymbol{u}^{*2}\rangle}\right)}l^2. \tag{41}$$

Re_λ^o is related to the number of grid points in each direction, N, and the spatial resolution determined by the dimensionless parameter $\kappa_{\max}\eta_k$ [23]. $\kappa_{\max}$ is the maximum wave number, and $\eta_k = (\nu^3/\varepsilon)^{1/4}$ is the Kolmogorov length scale. According to Yeung and Pope [24], $\kappa_{\max}\eta_k = 1.0$ is adequate for low-order velocity statistics, but at least $\kappa_{\max}\eta_k = 1.5$ is needed for higher order quantities such as dissipation. Since the current study examines higher order statistics as well as low-order ones, we want $\kappa_{\max}\eta_k \geqslant 1.5$. In a triply periodic DNS, $\kappa_{\max} = \pi N/L$. Then, the number of grid points is constrained by the Reynolds number.

$$N \geqslant \frac{1.5}{15^{\frac{1}{4}}\pi}\frac{L}{l}\text{Re}_\lambda^{o\,\frac{3}{2}}. \tag{42}$$

This relation has been used *a priori* to determine proper grid resolutions for DNS 1–4 in Sec. IV A.

Finally, the Reynolds number Re_D of the target experiment can be related to Re_λ of the DNS. Since the ratio $U_c x_o/\nu$ is proportional to the jet Reynolds number Re_D [21], $U_c x_o/\nu = C\text{Re}_D$, where C is a constant typically ranging from 5 to 7 in turbulent round jet experiments [19,20,25–28]. Then,

TABLE II. Relevant parameters of the target experiments and the corresponding simulations.

	Target experiments			Simulation parameters		
	$U_c[m/s]$	$x_o[m]$	Re_D	N	$L[m]$	Re_λ
DNS1	0.0796	0.232	3000	192	0.0932	76
DNS2	2.06	0.239	5500	256	0.0920	99
DNS3	1.36	0.732	11000	512	0.294	140
DNS4	1.95	1.60	37000	1024	0.640	255

it follows from Eq. (41) that

$$\mathrm{Re}_\lambda^o = \sqrt{\frac{45}{2} C \left(\frac{l}{x_o}\right)^2 \left(1 + \frac{\langle u_x^{*2}\rangle}{\langle \boldsymbol{u}^{*2}\rangle}\right) \mathrm{Re}_D}. \tag{43}$$

This form of relation in a turbulent jet, $\mathrm{Re}_\lambda \sim \mathrm{Re}_D^{1/2}$, was also suggested by Antonia *et al.* [29].

IV. RESULTS

A. Simulation framework and parameters

The governing equations, Eqs. (23)–(26), are solved using the NGA [30] code. NGA is a three-dimensional finite difference solver suitable for variable-density, low-Mach-number, laminar and turbulent flows. It solves the continuity and Navier-Stokes equations in physical space, not in spectral space, while discretely conserving kinetic energy. The Courant-Friedrichs-Lewy condition, CFL $\leqslant$ 0.8, has been imposed for all the simulations in the current paper.

The initial velocity fields are randomly generated, following the method used by Eswaran and Pope [11]. The velocity fields are subject to the continuity constraint and conformed to a specified Passot-Pouquet energy spectrum [31]. A detailed explanation can be found in [32].

Four simulations have been conducted at different Reynolds numbers. The relevant parameters are shown in Table II. The target experiment of DNS1 is Webster *et al.* [27]; DNS2, Vouros and Panidis [26]; DNS3, Panchapakesan and Lumley [19]; and DNS4, Antonia and Zhao [33]. Any experiment could be selected, but the limiting factor is the Reynolds number.

As stated in Sec. III D, U_c and x_o of each experiment are used to determine the domain width and forcing terms for the simulation. Re_λ is estimated *a priori* according to Eq. (41). Finally, N is determined according to Eq. (42).

B. Temporal fluctuations

After a transient period, the turbulence statistics under the linear forcing technique asymptotically reaches a unique solution [15]. Rosales and Meneveau noticed that the turbulent statistics are subject to large oscillations around their respective average values, even when the flow becomes statistically stationary. For the purpose of reducing the magnitudes of such oscillations while retaining the underlying physics, Carroll and Blanquart [2] proposed a modification to the linear forcing terms. Since the current study also uses linearly forcing terms, albeit anisotropic, the same modification is used for the simulations DNS 1–4:

(1) Longitudinal direction:

$$\frac{\varepsilon_o}{\left\langle k^* + \frac{u_x^{*2}}{2}\right\rangle} u_x^*. \tag{44}$$

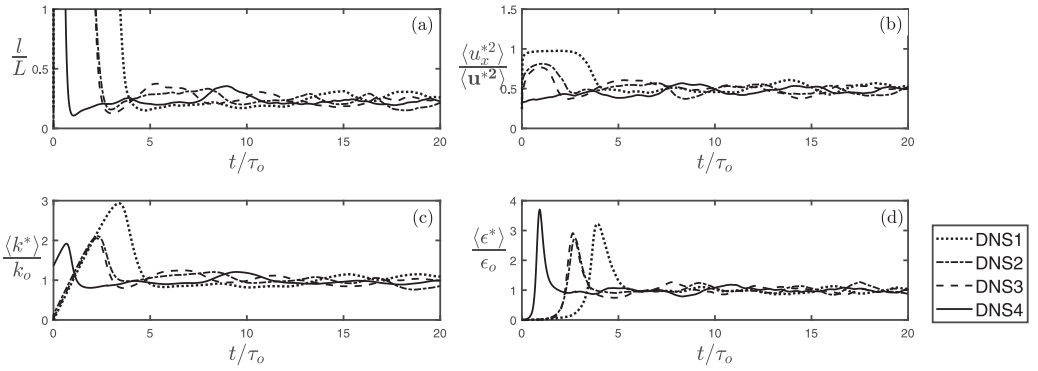

FIG. 1. Temporal fluctuations of turbulent parameters: (a) ratio of the integral length scale, l, to the domain width, L; (b) anisotropy $\langle u_x^{*2}\rangle/\langle \boldsymbol{u}^{*2}\rangle$; (c) the volume-averaged kinetic energy, $\langle k^*\rangle$, with respect to the expected value, k_o; (d) the volume-averaged dissipation rate, $\langle \varepsilon^*\rangle$, with respect to the expected value, ε_o. The parameters are plotted as a function of the time normalized by the *a priori* eddy time scale, τ_o.

(2) Transverse directions:

$$\frac{1}{2}\frac{\varepsilon_o}{\left\langle k^* + \frac{u_x^{*2}}{2}\right\rangle} u_i^*. \tag{45}$$

Figure 1 shows l, $\langle u_x^{*2}\rangle/\langle \boldsymbol{u}^{*2}\rangle$, $\langle k^*\rangle/k_o$, and $\langle \varepsilon^*\rangle/\varepsilon_o$, as a function of the normalized time, t/τ_o, where $\tau_o = k_o/\varepsilon_o$. τ_o is the eddy timescale determined *a priori*. The quantities are spatially averaged over the cubic box at each time step. All of the turbulent parameters reach statistical stationarity after a transient period. The length of the transient periods appears to depend on Re_λ; simulations with higher Re_λ have shorter transient periods. For DNS1 with $\mathrm{Re}_\lambda = 76$, stationary conditions are attained approximately at $t/\tau_o = 6$; for DNS 4 with $\mathrm{Re}_\lambda = 255$, $t/\tau_o = 3$.

The mean values of the turbulent parameters and the magnitudes of fluctuations over the statistically stationary periods are shown in Table III. The standard deviations are small enough to assume that the velocity fields have reached statistical stationarity.

The mean value of l/L is about 0.24, and the mean value of $\langle u_x^{*2}\rangle/\langle \boldsymbol{u}^{*2}\rangle$ is about 0.49. It indicates that the mean values of the two parameters are independent of Re_λ, despite the small variations. In addition, Figs. 1(c) and 1(d) display the temporal evolution of $\langle k^*\rangle$ and $\langle \varepsilon^*\rangle$ with their respective expected values. Regardless of Re_λ, the kinetic energy and dissipation rate indeed fluctuate around their expected values with relatively small amplitudes, when the system reaches statistical stationarity. Thus, it shows that the calculations for k_o and ε_o are quite accurate.

TABLE III. Mean values and standard deviations (Mean ± SD) of turbulent parameters over the statistically stationary region.

	l/L	$\langle u_x^{*2}\rangle/\langle \boldsymbol{u}^{*2}\rangle$	$\langle k^*\rangle/k_o$	$\langle \varepsilon^*\rangle/\varepsilon_o$
DNS1	0.238 ± 0.002	0.504 ± 0.002	0.986 ± 0.011	0.996 ± 0.006
DNS2	0.242 ± 0.002	0.493 ± 0.004	0.992 ± 0.012	1.009 ± 0.012
DNS3	0.239 ± 0.002	0.485 ± 0.003	1.002 ± 0.011	1.001 ± 0.007
DNS4	0.244 ± 0.002	0.490 ± 0.002	1.000 ± 0.008	0.991 ± 0.007

C. Validation against experimental data: Energy budget

We need to ensure that the simulation quantities, such as k^* and ε^*, are indeed equivalent to the experimental counterparts, k and ε. We start with the turbulent kinetic energy equation:

$$\begin{aligned} k &= \frac{1}{2}\boldsymbol{u}' \cdot \boldsymbol{u}'\Big|_{x=x_o} \\ &= \frac{1}{2}\left[\left(\frac{x_o}{x}e^{(\frac{x}{x_o}-1)}u_x^*\right)^2 + \left(\frac{x_o}{x}u_y^*\right)^2 + \left(\frac{x_o}{x}u_z^*\right)^2\right]\Big|_{x=x_o} \\ &= \frac{1}{2}\boldsymbol{u}^* \cdot \boldsymbol{u}^* = k^*. \end{aligned} \tag{46}$$

To examine the dissipation rate, let us consider the kinetic energy equation for the full jet derived from Eq. (7). Neglecting the pressure term and viscous diffusion, we can write the ensemble-averaged energy equation as

$$-\langle \boldsymbol{u}' \cdot \nabla \overline{\boldsymbol{u}} \cdot \boldsymbol{u}' \rangle - \overline{\boldsymbol{u}} \cdot \nabla \langle k \rangle - \nabla \cdot \langle \boldsymbol{u}' k \rangle - \overline{\varepsilon}_k = 0. \tag{47}$$

These four terms are named production, advection, diffusion, and dissipation terms from left to right [19]. The production term is the same for experiment and simulation:

$$-\langle \boldsymbol{u}' \cdot \nabla \overline{\boldsymbol{u}} \cdot \boldsymbol{u}' \rangle|_{x=x_o} = -\langle \boldsymbol{u}^* \cdot \nabla \overline{\boldsymbol{u}} \cdot \boldsymbol{u}^* \rangle \tag{48}$$

$$= \frac{U_c}{x_o}k_o\left(3\frac{\langle u_x'^2 \rangle}{\langle \boldsymbol{u}'^2 \rangle} - 1\right). \tag{49}$$

For the advection term, we only apply the *advection normalization*, because *continuity normalization* is a mathematical technique to make the flow divergence free and therefore should not be related to the advection term. Then,

$$-\overline{\boldsymbol{u}} \cdot \nabla \langle k \rangle|_{x=x_o} = -\overline{\boldsymbol{u}} \cdot \nabla \left\langle \frac{x_o^2}{x^2}k^* \right\rangle\Big|_{x=x_o} \tag{50}$$

$$= \overline{\boldsymbol{u}} \cdot \cancel{\nabla \langle k^* \rangle} + 2\frac{U_c}{x_o}k_o. \tag{51}$$

The diffusion term is zero for both experiments and simulations, because these third-order moments are zero:

$$-\nabla \cdot \langle \boldsymbol{u}' k \rangle|_{x=x_o} = -\nabla \cdot \cancel{\langle \boldsymbol{u}^* k^* \rangle} + \frac{3}{2x_o}\cancel{\langle u_x^* k^* \rangle} = 0. \tag{52}$$

Finally, the dissipation term is simply the negation of the sum of the other terms:

$$\begin{aligned} \overline{\varepsilon}_k|_{x=x_o} &= -(\overline{\boldsymbol{u}} \cdot \nabla \langle k \rangle + \langle \boldsymbol{u}' \cdot \nabla \overline{\boldsymbol{u}} \cdot \boldsymbol{u}' \rangle + \nabla \cdot \langle \boldsymbol{u}' k \rangle)|_{x=x_o} \\ &= \frac{U_c}{x_o}k_o\left(1 + 3\frac{\langle u_x'^2 \rangle}{\langle \boldsymbol{u}'^2 \rangle}\right). \end{aligned} \tag{53}$$

With the expression for k_o from Eq. (33) and $\langle u_x'^2 \rangle / \langle \boldsymbol{u}'^2 \rangle \approx 0.49$ from Eq. (36), these four terms are directly compared against experimental values of Panchapakesan and Lumley [19] in Fig. 2. Each term is normalized by $U_c^3/r_{1/2}$. The half-width of a round jet, $r_{1/2}$, is the radial distance where the axial velocity is $\frac{1}{2}U_c$. According to Panchapakesan and Lumley, $r_{1/2} = 0.096x_o$. Since the target flow of the current study is the centerline region of a round jet, the estimated values for each term are plotted as points at $\eta = 0$. Despite small differences, all of the four terms agree well with the experimental measures.

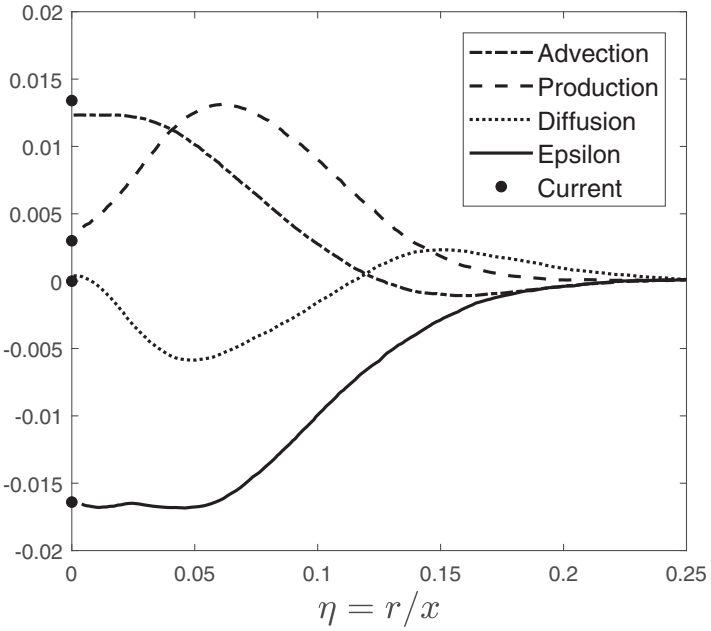

FIG. 2. Energy budget comparison. Each term is normalized by $U_c^3/r_{1/2}$. The lines are experimental data from Ref. [19], and the points are the estimated values from Eqs. (48)–(53).

Note that the expression for $\overline{\varepsilon}_k$ in Eq. (53) is different from the expression for ε_o in Eq. (34). The difference is caused by the *continuity normalization*, which creates an extra term through $\overline{\boldsymbol{u}} \cdot \nabla \langle k \rangle$. In other words, ε_k is equivalent to the sum of $\varepsilon_o = 2\nu S_{ij}^* S_{ij}^*$ computed from our DNS and the additional term from the *continuity normalization*; i.e.,

$$\overline{\varepsilon}_k = \varepsilon_o + 2\frac{U_c}{x_o} k_o \left(\frac{\langle u_x'^2 \rangle}{\langle \boldsymbol{u'^2} \rangle} \right). \tag{54}$$

D. Validation against experimental data: Single point values

As demonstrated in Secs. IV B and IV C, the following values are the results of the DNS with the present source term:

$$\frac{k_o}{U_c^2} \approx 0.0698, \tag{55}$$

$$\frac{\varepsilon_k}{U_c^3/x_o} \approx 0.171. \tag{56}$$

The three normalized scalar quantities, $\frac{\langle u_x'^2 \rangle}{\langle \boldsymbol{u'^2} \rangle}$, $\frac{k}{U_c^2}$, and $\frac{\varepsilon_k}{U_c^3/x_o}$, are plotted as a function of Re_D in Fig. 3. Boersma(98) and Boersma(04) are DNS data, and the rest are experiments. A dashed line is used to represent values of the current study for all the Reynolds numbers, since the results are independent of the Reynolds number. For the energy dissipation rate, ε_k is used instead of ε_o, because ε_k is the quantity equivalent to the dissipation in experiments.

One should first acknowledge that the published values do not completely agree with one another, even among experiments or computations. Instead, there seem to be some ranges of values for the respective parameters: 0.40–0.58 for $\frac{\langle u_x'^2 \rangle}{\langle \boldsymbol{u'^2} \rangle}$; 0.05–0.09 for $\frac{k}{U_c^2}$; and 0.08–0.23 for $\frac{\varepsilon_k}{U_c^3/x_o}$. Possible reasons for these differences include the state of the boundary layer on the nozzle wall, differences in

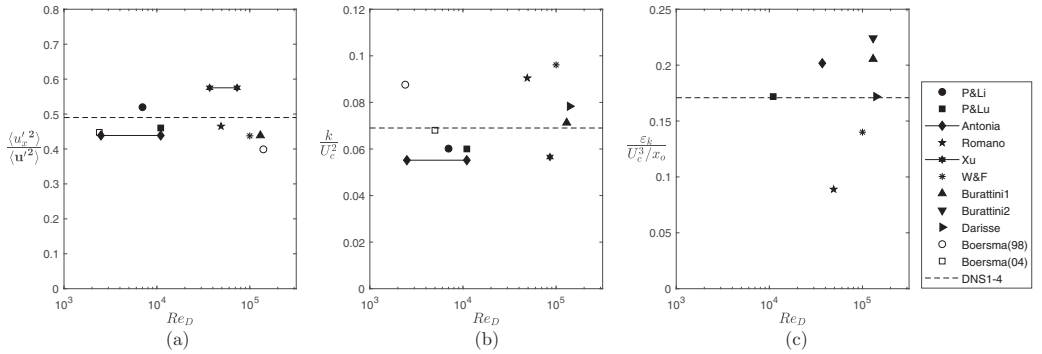

FIG. 3. Single-point values comparison: (a) anisotropy $\frac{\langle u_x'^2\rangle}{\langle \boldsymbol{u'^2}\rangle}$; (b) normalized kinetic energy $\frac{k}{U_c^2}$; (c) normalized dissipation rate $\frac{\varepsilon_k}{U_c^3/x_o}$. Boersma(98) [34] and Boersma(04) [35] are DNS. P&Li [36], P&Lu [19], Antonia [33], Romano [28], Xu [18], W&F [25], Burattini [17], and Darisse [22] are experiments.

the experimental techniques, and different ways to estimate derivatives. The value of each parameter for the current study lies within its respective range. Lundgren's forcing scheme would have $\frac{\langle u_x'^2\rangle}{\langle \boldsymbol{u'^2}\rangle} = 0.33$, below the experimental values.

In addition, the origins of the forcing term are examined again in Fig. 4. *Mean* only uses the forcing term from $\nabla\overline{\boldsymbol{u}}$. Thus, the forcing term is the first column of Table I: $\boldsymbol{f} = \frac{U_c}{x_o}\langle u_x, -\frac{1}{2}u_y, -\frac{1}{2}u_z\rangle$. *Mean+Adv* uses the forcing term from $\nabla\overline{\boldsymbol{u}}$ and the advection normalization; thus, the forcing term is the sum of the first and second columns of Table I: $\boldsymbol{f} = \frac{U_c}{x_o}\langle 2u_x, \frac{1}{2}u_y, \frac{1}{2}u_z\rangle$. *All* uses the original forcing term derived in Sec. III B.

The time-averaged values from $10\tau_o$ to $50\tau_o$ are displayed in Table IV. Also, the ranges for the experimental values are shown. Among the three forcing terms, only the original *All* forcing produces the turbulent characteristics of round jets correctly. These plots and table help to show that the two normalizations are essential to create the right turbulence.

E. Validation against experimental data: Energy spectra

The energy spectrum is compared against the experiment of Burattini *et al.* [17]. The one-dimensional energy spectrum, $\phi(\kappa_1)$, is defined as

$$\int_0^\infty \phi(\kappa_1)d\kappa_1 = k, \tag{57}$$

where κ_1 is the wave number in the longitudinal direction. $\phi(\kappa_1)$ is the Fourier-transformed function of the spatial correlation function $\langle \boldsymbol{u'}(\boldsymbol{x})\cdot\boldsymbol{u'}(\boldsymbol{x}+\boldsymbol{r_1})\rangle$, where $\langle\cdot\rangle$ is the volumetric averaging, and $\boldsymbol{r_1}$ is a vector in the longitudinal direction.

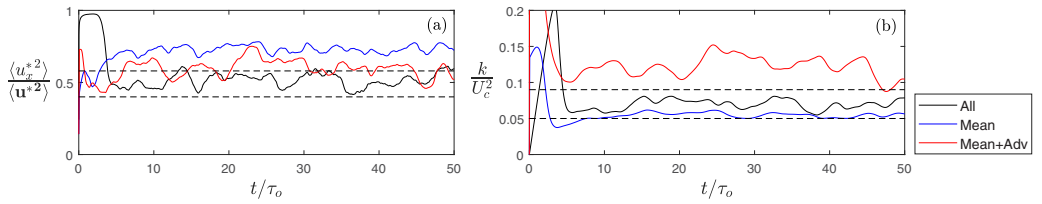

FIG. 4. Examination of the origins of the forcing term: (a) anisotropy $\frac{\langle u_x^{*2}\rangle}{\langle \boldsymbol{u^{*2}}\rangle}$; (b) normalized kinetic energy $\frac{k}{U_c^2}$. The parameters are plotted as a function of the time normalized by the *a priori* eddy timescale, τ_o. *All* (black) refers to the original forcing term; *Mean* (blue), the forcing term from $\nabla\overline{\boldsymbol{u}}$ only; and *Mean+Adv* (red), the forcing term from $\nabla\overline{\boldsymbol{u}}$ and advection normalization.

TABLE IV. Examination of the origins of the forcing term: time-averaged values of turbulent parameters.

	$\langle u_x^{*2}\rangle/\langle \boldsymbol{u}^{*2}\rangle$	k/U_c^2
All	0.49	0.070
Mean	0.73	0.056
Mean+Adv	0.60	0.12
Experiments	0.40–0.58	0.05–0.09

This spatial energy spectrum, $\phi(\kappa_1)$, can be easily computed in the triply periodic DNS. Since the governing equations in this study are in the Lagrangian reference frame, the spatial energy spectrum of our DNS can be compared to the temporal energy spectrum of an experiment, which assumes Taylor's frozen turbulence hypothesis [37]. The energy spectra from Burattini *et al.* and DNS4 are displayed in Fig. 5. The two spectra agree with each other very well in the inertial-convective subrange as well as in the dissipative subrange. The small deviation in the high-wave-number region may be caused by the estimation of η in the experiment.

Burattini *et al.* obtained the relation, $\phi \sim \kappa^{-1.52}$, by using a least squares fit to the spectrum in the inertial subrange. We use the following model spectrum from Pope [16] to determine the power-law scaling:

$$\phi(\kappa) = \alpha \varepsilon^{2/3} \kappa^{-n} f_L(\kappa L) f_\eta(\kappa \eta_k), \tag{58}$$

$$f_\eta(\kappa \eta_k) = \exp\left(-\beta\left[\left((\kappa \eta_k)^4 + c_\eta^4\right)^{1/4} - c_\eta\right]\right), \tag{59}$$

$$f_L(\kappa L) = \left(\frac{\kappa L}{((\kappa L)^2 + c_L)^{1/2}}\right)^{11/3}, \tag{60}$$

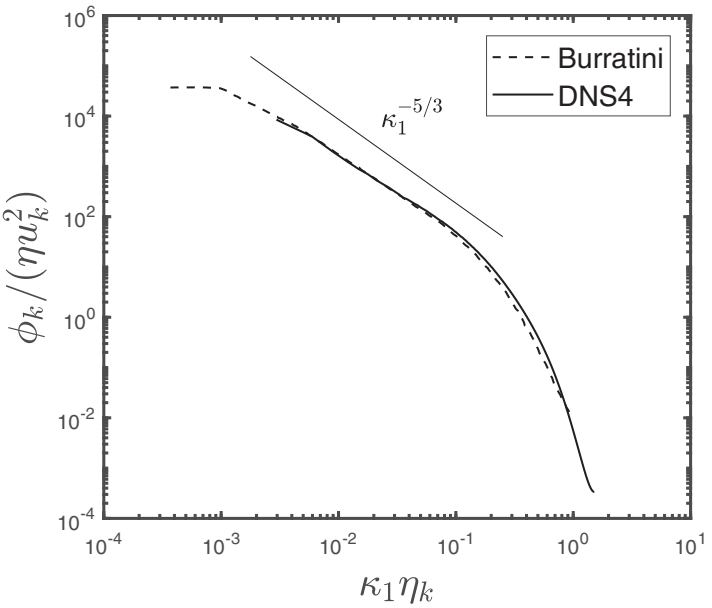

FIG. 5. Comparison of normalized kinetic energy spectra in the longitudinal direction. $u_k = (\nu\varepsilon)^{1/4}$ is the Kolmogorov velocity scale.

where α is a constant and $L = k^{3/2}/\varepsilon$. For high Reynolds numbers, $c_\eta = 0.2, \beta = 4.7,$ and $c_L = 6.78$ should be appropriate, according to Pope [16]. A least-squares fit is used over the inertial subrange and the dissipation range with Eq. (58) to determine $C = 2.69$ and $n = 1.50$.

The scalings from Burattini *et al.* and our study are very close to each other, different from the high-Reynolds-number theoretical prediction of Kolmogorov [38]. The Reynolds numbers of both Burattini's experiment and DNS4 might not be high enough to reach $n = -5/3$, which is obtained as a result of assuming a very large Re.

V. CONCLUSION

Existing forcing schemes are numerical methods that successfully prevent the turbulence from decaying, but they were not derived by using the information of a specific flow. In contrast, the purpose of this work was to derive a forcing technique based on the physical properties of a practical turbulent flow. Reynolds decomposition with the mean velocity of a turbulent round jet was used to find the momentum equations for the fluctuating velocity. The resulting forcing terms are found to be anisotropic linear forcing terms in physical space.

First, the anisotropy $\langle u_x'^2 \rangle / \langle \boldsymbol{u'^2} \rangle$, kinetic energy k, and dissipation rate ε_k were compared against multiple experiments. DNS results were found to be within the range of experimental values. Then, the energy budget terms were compared against experimental values at the centerline of a turbulent round jet. Finally, the spectrum computed from the DNS data of the current study agrees well with that of Burattini *et al.*, including the scaling of about $\kappa^{-1.5}$ in the inertial-convective region. Thus, it seems appropriate to conclude that the proposed forcing terms successfully produce the turbulent characteristics of a turbulent round jet in a triply periodic box.

The essence of this work is to show the possibility that a forcing technique (for 3D periodic box turbulence) can be based on the physics of a practical flow, instead of being an arbitrary numerical method as all the previous ones. The current forcing term is focused on the centerline of a jet in the self-similar region. It is also developed to be used only in a 3D periodic box of turbulence. We developed a forcing scheme for this local area on purpose, so that the forcing terms are simple and clear. By using similar derivation methods, however, more forcing terms can be discovered for different flow geometries.

ACKNOWLEDGMENTS

The authors gratefully acknowledge funding from the National Science Foundation (CBET 1512771) and from the Air Force Office of Scientific Research (FA9550-16-1-0510) under the supervision of Dr. Chiping Li. In addition, K.J.R. acknowledges the financial support from the Samsung Scholarship Foundation.

[1] P. L. Carroll, S. Verma, and G. Blanquart, A novel forcing technique to simulate turbulent mixing in a decaying scalar field, Phys. Fluids **25**, 095102 (2013).

[2] P. L. Carroll and G. Blanquart, A proposed modification to Lundgren's physical space velocity forcing method for isotropic turbulence, Phys. Fluids **25**, 105114 (2013).

[3] S. Ghosal, T. S. Lund, P. Moin, and K. Akselvoll, A dynamic localization model for large-eddy simulation of turbulent flows, J. Fluid Mech. **286**, 229 (1995).

[4] D. Carati, S. Ghosal, and P. Moin, On the representation of backscatter in dynamic localization models, Phys. Fluids **7**, 606 (1995).

[5] J. R. Chasnov, Simulation of the Kolmogorov inertial subrange using an improved subgrid model, Phys. Fluids A **3**, 188 (1991).

[6] N. P. Sullivan, S. Mahalingam, and R. M. Kerr, Deterministic forcing of homogeneous, isotropic turbulence, Phys. Fluids **6**, 1612 (1994).

[7] C. Seror, P. Sagaut, C. Bailly, and D. Juvé, On the radiated noise computed by large-eddy simulation, Phys. Fluids **13**, 476 (2001).
[8] B. Savard, B. Bobbitt, and G. Blanquart, Structure of a high Karlovitz n-C_7H_{16} premixed turbulent flame, Proc. Combust. Inst. **35**, 1377 (2015).
[9] A. Y. Poludnenko and E. S. Oran, The interaction of high-speed turbulence with flames: Global properties and internal flame structure, Combust. Flame **157**, 995 (2010).
[10] P. E. Hamlington, A. Y. Poludnenko, and E. S. Oran, Intermittency in premixed turbulent reacting flows, Phys. Fluids **24**, 075111 (2012).
[11] V. Eswaran and S. B. Pope, An examination of forcing in direct numerical simulations of turbulence, Comput. Fluids **16**, 257 (1988).
[12] N. Wax, *Selected Papers on Noise and Stochastic Processes* (Courier Dover, New York, 1954).
[13] K. Alvelius, Random forcing of three-dimensional homogeneous turbulence, Phys. Fluids **11**, 1880 (1999).
[14] T. S. Lundgren, Linearly forced isotropic turbulence, in *Annual Research Briefs* (Center for Turbulence Research, Stanford, 2003), pp. 461–473.
[15] C. Rosales and C. Meneveau, Linear forcing in numerical simulations of isotropic turbulence: Physical space implementations and convergence properties, Phys. Fluids **17**, 095106 (2005).
[16] S. B. Pope, *Turbulent Flows* (Cambridge University Press, Cambridge, 2001).
[17] P. Burattini, R. A. Antonia, and L. Danaila, Similarity in the far field of a turbulent round jet, Phys. Fluids **17**, 025101 (2005).
[18] G. Xu and R. Antonia, Effect of different initial conditions on a turbulent round free jet, Exp. Fluids **33**, 677 (2002).
[19] N. R. Panchapakesan and J. L. Lumley, Turbulence measurements in axisymmetric jets of air and helium. Part 1. Air jet, J. Fluid Mech. **246**, 197 (1993).
[20] H. J. Hussein, S. P. Capp, and W. K. George, Velocity measurements in a high-Reynolds-number, momentum-conserving, axisymmetric, turbulent jet, J. Fluid Mech. **258**, 31 (1994).
[21] G. N. Abramovich, *The Theory of Turbulent Jets* (MIT Press, Cambridge, 1963).
[22] A. Darisse, J. Lemay, and A. Benaïssa, Budgets of turbulent kinetic energy, Reynolds stresses, variance of temperature fluctuations and turbulent heat fluxes in a round jet, J. Fluid Mech. **774**, 95 (2015).
[23] P.-K. Yeung and S. B. Pope, Lagrangian velocity statistics obtained from direct numerical simulations of homogeneous turbulence, in *6th Symposium on Turbulent Shear Flows* (Springer-Verlag, Berlin, 1987), pp. 3–7.
[24] P.-K. Yeung and S. B. Pope, Lagrangian statistics from direct numerical simulations of isotropic turbulence, J. Fluid Mech. **207**, 531 (1989).
[25] I. Wygnanski and H. Fiedler, Some measurements in the self-preserving jet, J. Fluid Mech. **38**, 577 (1969).
[26] A. P. Vouros and T. Panidis, Turbulent properties of a low Reynolds number, axisymmetric, pipe jet, Exp. Therm. Fluid Sci. **44**, 42 (2013).
[27] D. R. Webster, P. J. W. Roberts, and L. Ra'ad, Simultaneous DPTV/PLIF measurements of a turbulent jet, Exp. Fluids **30**, 65 (2001).
[28] G. P. Romano and R. A. Antonia, Longitudinal and transverse structure functions in a turbulent round jet: Effect of initial conditions and Reynolds number, J. Fluid Mech. **436**, 231 (2001).
[29] R. A. Antonia, B. R. Satyaprakash, and F. Hussain, Measurements of dissipation rate and some other characteristics of turbulent plane and circular jets, Phys. Fluids **23**, 695 (1980).
[30] O. Desjardins, G. Blanquart, G. Balarac, and H. Pitsch, High order conservative finite difference scheme for variable density low Mach number turbulent flows, J. Comput. Phys. **227**, 7125 (2008).
[31] T. Passot and A. Pouquet, Numerical simulation of compressible homogeneous flows in the turbulent regime, J. Fluid Mech. **181**, 441 (1987).
[32] P. L. Carroll, Towards understanding the mixing characteristics of turbulent buoyant flows, Ph.D. thesis, California Institute of Technology, 2014 (unpublished).
[33] R. A. Antonia and Q. Zhao, Effect of initial conditions on a circular jet, Exp. Fluids **31**, 319 (2001).
[34] B. J. Boersma, G. Brethouwer, and F. T. M. Nieuwstadt, A numerical investigation on the effect of the inflow conditions on the self-similar region of a round jet, Phys. Fluids **10**, 899 (1998).

[35] B. J. Boersma, Numerical simulation of the noise generated by a low Mach number, low Reynolds number jet, Fluid Dyn. Res. **35**, 425 (2004).

[36] P. N. Papanicolaou and E. J. List, Investigations of round vertical turbulent buoyant jets, J. Fluid Mech. **195**, 341 (1988).

[37] G. I. Taylor, The spectrum of turbulence, Proc. R. Soc. London A **164**, 476 (1938).

[38] A. N. Kolmogorov, The local structure of turbulence in incompressible viscous fluid for very large Reynolds numbers, Dokl. Akad. Nauk SSSR **434**, 9 (1991).